AppliedMath

MDPI

Article

Urban Geography Compression Patterns: Non-Euclidean and Fractal Viewpoints

Daniel A. Griffith [1,*] and Sandra Lach Arlinghaus [2,*]

[1] School of Economic, Political, and Policy Sciences, University of Texas at Dallas, Richardson, TX 75080, USA
[2] School for Environment and Sustainability, The University of Michigan, Ann Arbor, MI 48109, USA
* Correspondence: dagriffith@utdallas.edu (D.A.G.); sarhaus@umich.edu (S.L.A.)

Abstract: The intersection of fractals, non-Euclidean geometry, spatial autocorrelation, and urban structure offers valuable theoretical and practical application insights, which echoes the overarching goal of this paper. Its research question asks about connections between graph theory adjacency matrix eigenfunctions and certain non-Euclidean grid systems; its explorations reflect accompanying synergistic influences on modern urban design. A Minkowski metric with an exponent between one and two bridges Manhattan and Euclidean spaces, supplying an effective tool in these pursuits. This model coalesces with urban fractal dimensions, shedding light on network density and human activity compression. Unlike Euclidean geometry, which assumes unique shortest paths, Manhattan geometry better represents human movements that typically follow multiple equal-length network routes instead of unfettered straight-line paths. Applying these concepts to urban spatial models, like the Burgess concentric ring conceptualization, reinforces the need for fractal analyses in urban studies. Incorporating a fractal perspective into eigenvector methods, particularly those affiliated with spatial autocorrelation, provides a deeper understanding of urban structure and dynamics, enlightening scholars about city evolution and functions. This approach enhances geometric understanding of city layouts and human behavior, offering insights into urban planning, network density, and human activity flows. Blending theoretical and applied concepts renders a clearer picture of the complex patterns shaping urban spaces.

Keywords: Burgess model; fractal; Manhattan metric; Minkowski metric; non-Euclidean geometry

Academic Editor: Chengxi Zhang

Received: 17 December 2024
Revised: 8 January 2025
Accepted: 13 January 2025
Published: 21 January 2025

Citation: Griffith, D.A.; Arlinghaus, S.L. Urban Geography Compression Patterns: Non-Euclidean and Fractal Viewpoints. *AppliedMath* **2025**, *5*, 9. https://doi.org/10.3390/appliedmath5010009

1. Introduction

There is considerable interest in the fractal (e.g., [1]) dimensions (e.g., [2]) of networks (e.g., [3–13]). Its sizeable literature has reached the critical mass that prompts academics now to write comprehensive literature reviews about fractals for specialized areas (e.g., [14]), including their use in urban planning (e.g., [15,16]). The same scenario is beginning to emerge for their complexity theory relative too (e.g., [17]), sometimes with special emphasis on such facets as urban morphology (e.g., [18]) and urban spatial complexity (e.g., [19]). In addition, some of the literature addresses relationships between graph spectra and fractal dimensions (e.g., [20,21]), a clue that one of its cognate scholastic fields is spatial autocorrelation. Synthesizing and extending these ideas, Griffith and Arlinghaus [22] furnish a brief history and a conceptual overview of the problem of geographic network space fractal dimensions, and whether or not Euclidean geometry should capitulate to non-Euclidean geometry (e.g., [23,24]) as the two-dimensional geometric space supporting geographical theories. This paper furnishes foundational technical and theoretical sustenance for their

conceptual framework, deferring a comprehensive literature review to those publications already existing and cited in this paragraph.

A fractal may be defined as a set for which the Hausdorff–Besicovitch dimension (e.g., [25]), which can be non-integer, strictly exceeds its topological dimension. Its precise computation can be made with the box-counting method (e.g., [26]), which is applicable to two-dimensional images as follows (after [27]):

Definition 1. *For geographic/geometric resolution extent $1/2^k$, the argument in $N(1/2^k)$ denoting a count of the minimum number of squares/boxes of side-length 2^k needed to cover all of the lines forming a two-dimensional image, the Hausdorff–Besicovitch dimension, d, is given by*

$$d = \lim_{k \to \infty} \frac{LN\left[N\left(1/2^k\right)\right]}{k\, LN(2)},$$

where LN denotes the natural logarithm. The dimension d calculated as the solution to this limit is always at least as large as its topological counterpart.

Manhattan (also known as city block or taxicab—a name coined by Karl Menger in 1952; e.g., [28–33]; also see [34]) geometry is a geometric model conceptually introduced in the 19th century by two mathematicians, Lithuanian Hermann Minkowski (i.e., his conceptions of grid-based distance and metric systems laying its groundwork) and Hungarian Frigyes Riesz; this latter scholar is credited with formalizing it as L_p—more specifically L_1—space, adopting linear algebra nomenclature. Manhattan geometry constitutes one category of non-Euclidean geometry that replaces the Pythagorean theorem with a metric that equals the sum of the absolute values of the differences (i.e., the distance exponent is 1, the value of *p*)—rather than the square root of the sums of these differences squared, or L_2—between each pair of two-dimensional coordinates' georeferencing points. Summing the absolute differences of such point coordinate pairs along each of two orthogonal axes is mathematically equivalent to the L_1-norm in linear algebra (i.e., the sum of the absolute values of a vector's components), which aligns perfectly with measuring straight-path distance while navigating the street grid of Manhattan, New York, spawning its name. Moreover, the plane can have a square grid superimposed upon it, resulting in a regular square grid of points. This geometric space may be defined as follows (e.g., [35]; after [36]):

Definition 2. *A two-dimensional Manhattan space comprises n^2 points (u_i, v_i), $u_i = 1, 2, \ldots, n$ and $v_i = 1, 2, \ldots, n$ and $i = (v_i - 1)n + u_i$, forming an n-by-n regular square mesh grid, whose mesh cell side linking pairs of nearby points measures exactly one separation unit apart, resulting in a regular square tessellation plane geometry figure coupled with an attendant regular square lattice graph. Similarly, central place geometry is non-Euclidean and also replaces the Pythagorean theorem with a metric equaling the shortest path between two points along arcs of a hexagonal lattice. This space may be defined as follows, encapsulating the preceding distance definition (see [37]; after [38,39]).*

Definition 3. *A two-dimensional central place geometric space comprises n^2 points (u_i, v_i), $u_i = 1, 2, \ldots, n$ and $v_i = 1, 2, \ldots, n$ and $i = (v_i - 1)(2n - 1)/2 + u_i$ for odd v_i and $i = v_i(2n - 1)/2 - n + 1 + u_i$ for even v_i, forming a regular hexagonal n-by-n grid (e.g., even v_j integer rows of points are located at u_i integer values, whereas odd v_j integer rows of points are replaced by their integer values times $\left(\sqrt{3}\right)/2$ and located at the midpoint between the integer u_i values), whose polygon side linking pairs of nearby points measures exactly one separation unit apart, resulting in a regular hexagonal tessellation plane geometry figure coupled with an attendant regular hexagonal lattice graph. These are only two of a variety of regular polygon possibilities*

(e.g., [40]), such as ones constructed with identical isosceles triangles or rhombuses with only two distinct non-90° angles [41] (especially Figure 1). These two lattices are, respectively, related to the two preceding ones, with Kurlin [41] (§5) formally defining their metrics (subject to prevailing isometry, rigid motion, and similarity properties).

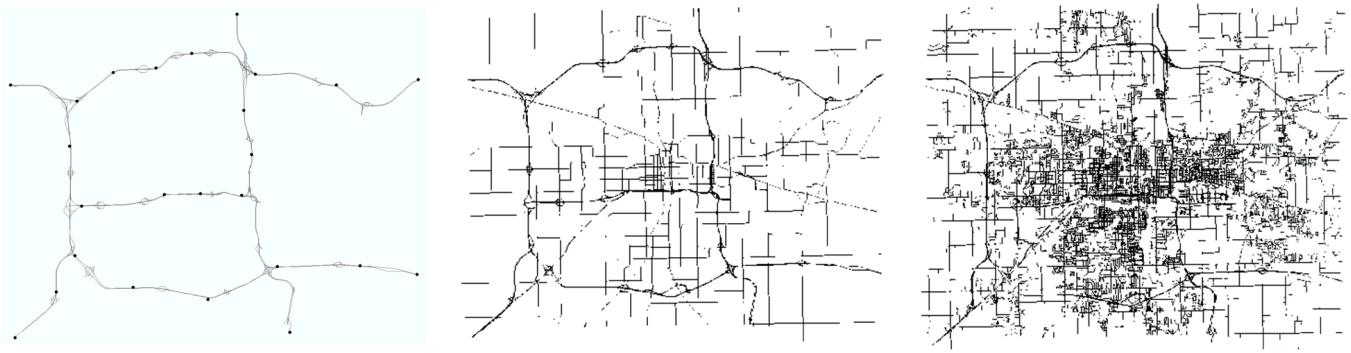

(**a**) (**b**) (**c**)

Figure 1. Arterial network structure in the Lansing, MI, metropolitan region, 2009. Left (**a**): expressways. Middle (**b**): (**a**) plus highways. Right (**c**): (**b**) plus streets.

Consequently, the primary objective of this paper is to summarize results for unit-square-based analyses upon which the density of a lattice grid increases. In doing so, it engages the following research question: What can be said about the interface between fractal dimensions, non-Euclidean metrics, and spatial autocorrelation eigenvectors? Empirical examples motivate this exploration, and, in doing so, integrate fractals, non-Euclidean geometric spaces (e.g., [42]), and spatial statistics. The fractal dimension calculator utilized in this paper is the Fractalyse 2.4 software (NOTE: fractal dimensions calculated for the following images supply a benchmark for comparative purposes: a straight line, Sierpiński carpet, a Koch coastline, a Koch island, a Sierpiński gasket, and a filled rectangle). It is a box-counting algorithm implementation for computing fractal dimensions selected because (1) this research is broad and interdisciplinary, suggesting that conceptually intuitive and easy-to-comprehend techniques are preferable, and (2) more importantly, the real-world settings investigated in this paper together with guidance from reality, which are the two crucial factors that should dictate tool selection, suggest the use of this computational procedure, rather than the other way around. This second point reflects a focus on the existing Chicago street layout (and the geometric Burgess model it germinated), which mostly follows a grid pattern, and which in turn aligns with the cells in the box-counting measurement. In contrast, spotlighting neighborhood rather than transportation structure, for example, would have prompted a computational procedure based upon spheres or circles, a fractal tool selection guided by the general multiple nuclei model of Harris and Ullman, with special reference to Chicago neighborhood compositions that exhibit adjacent well-defined polygons. In other words, the adopted box-counting procedure constitutes a more customized tool fit for both the chosen empirical conditions and their affiliated classic model description, letting the geography of a situation be the choice guide.

In keeping with the aforementioned objective, the scope of this paper spans formal mathematical results about actual as well as abstract two-dimensional networks that are self-similar at different scales while possessing differing geometric and fractal dimensions, supplementing simpler rectangular with more complicated hexagonal lattice configurations, ultimately relating fractal dimensions to network graph adjacency matrix principal eigenvectors as well as salient facets of spatial autocorrelation. Accordingly,

it addresses complexity issues by exploiting an analytical framework for studying and understanding urban spatial structures that are made up of interacting fractal, non-Euclidean metric, and spatial autocorrelation mechanisms, where the collective behavior of these three ingredients is often surprising, unpredictable, and not easily reducible to the sum of their individual analysis findings (see [43–47]). Therefore, the important contribution made here concerns the interplay between systematic spatial trends and fractal geometry that together can generate certain spatial autocorrelation patterns, and, in some cases, a higher fractal dimension, which in turn can indicate more complex spatial organizations, which then might show yet higher levels of spatial autocorrelation, jointly yielding a better understanding of relationships between these two concepts, an important goal of science.

2. Empirical Evidence

Analysis of selected real-world transportation networks and surface partitionings yields empirical evidence implying that physical space is non-Euclidean in nature. Griffith et al. [48] analyze minimum network paths between selected points in the hierarchical set of expressways, highways, and streets for the Lansing, MI, metropolitan region (Figure 1) and minimum network paths between all stations in four selected limited-access urban mass-transit rail networks (Figure 2)—namely, Pittsburgh, Dallas–Ft. Worth, Toronto, and Washington, DC—and find that, based upon estimated Minkowski metric function parameters, the Manhattan metric L_1-norm provides the best characterization of these minimum paths. Execution of this exercise involved a nonlinear regression of inter-point distances, the response variable, on the distance formula with given (u_i, v_i), $i = 1, 2, \ldots, n$, coordinates and unknown exponent parameters; the number of observations was the number of distance pairs, namely $n(n + 1)/2$. Furthermore, the restricted-access expressway distance formula yielded an exponent estimate that more closely resembles a Manhattan metric (i.e., it is relatively close to one), whereas the estimated distance expression for the combination of all three types of roads is approximately the midpoint between a Manhattan and a Euclidean metric (i.e., it is relatively close to 1.5). These researchers supplement their exploratory work with an analysis of minimum paths between residential houses and arterial road exits in two limited-access neighborhoods (Figure 3) located in the Lansing, MI, metropolitan region—namely, Whitehills and Bailey—and obtain the same implications.

(**a**) (**b**) (**c**) (**d**)

Figure 2. Mass-transit rail systems. Left (**a**): Pittsburgh light rail T. Left middle (**b**): Toronto subway system. Right middle (**c**): Dallas–Ft. Worth DART. Right (**d**): Washington, DC, subway.

The centroids of selected surface partitionings were used to construct dual graphs for these polygons. In order to improve network type coverage, five ideal planar graphs—namely, a straight line with endpoints, a triangle, a K4 complete planar graph, a balloon graph, and a dodecahedral graph—supplement these empirical surface dual graphs.

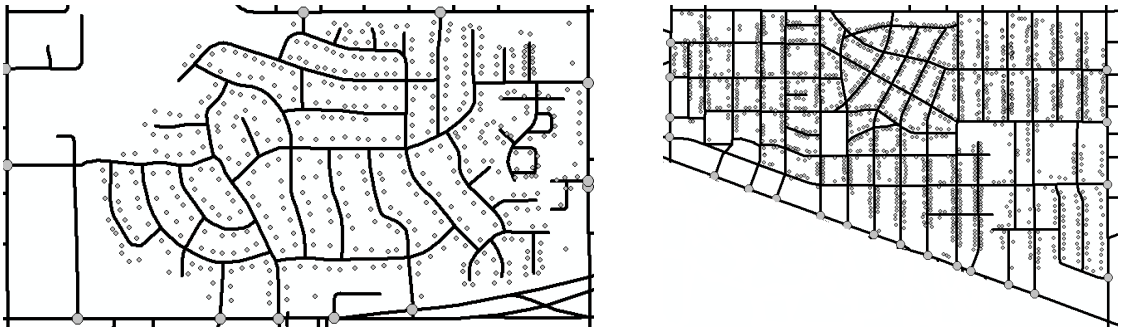

(**a**) (**b**)

Figure 3. Lansing, MI, limited-access residential neighborhoods; small gray dots denote houses, and large gray dots denote arterial road exit locations. Left (**a**): Whitehills. Right (**b**): Bailey.

3. Manhattan Space: Infill Asymptotics

One of the simplest forms of a Manhattan space is a square with four points. If these points and the four links among them align with the borders and corners of a unit square, Manhattan spaces can be created by—usually simultaneously and symmetrically—adding more vertical and horizontal lines between these border linkages. As the number of lines increases infinitely, the resulting Manhattan space lattice grid gradually converges to a fully filled-in unit square (Figure 4).

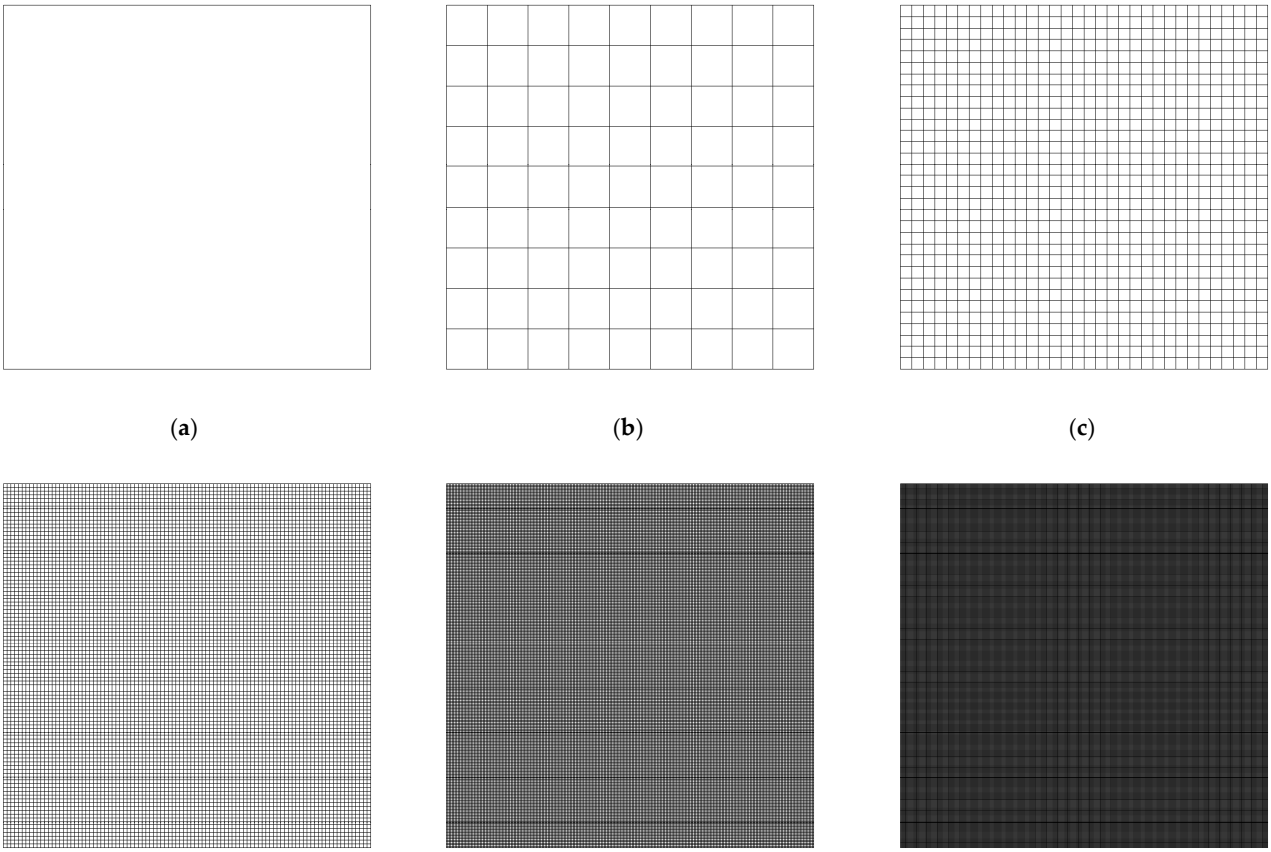

(**a**) (**b**) (**c**)

(**d**) (**e**) (**f**)

Figure 4. Manhattan space with increasing n. Top left (**a**): $n = 2$. Top middle (**b**): $n = 10$. Top right (**c**): $n = 33$. Bottom left (**d**): $n = 99$. Bottom middle (**e**): $n = 197$. Bottom right (**f**): $n = 400$.

3.1. Lattice-Based Matrix Algebra Results

The regular square lattice graph representation of a Manhattan space is reminiscent of regular square tessellations appearing in spatial statistics (e.g., remotely sensed image pixels and experimental agricultural field plots). Consequently:

Lemma 1. *A planar graph that is a regular square lattice of n^2 points forming an n-by-n square region has the principal eigenvalue for its corresponding 0–1 binary adjacency matrix (with diagonal values of 0) of $\lambda_1 = 4COS[\pi/(n+1)]$.*

Proof. See [49]. □

The inverse of this eigenvalue denotes the maximum value of positive spatial autocorrelation for a feasible spatial autoregressive model, namely 1/4.

Lemma 2. $\underset{n\to\infty}{limit} 4COS[\pi/(n+1)] = 4.$

Proof. As n approaches infinity, $\pi/(n+1)$ approaches 0.

$COS(0) = 1$

$4 \times 1 = 4$. □

In other words, the principal eigenvalue of the adjacency matrix, **C**, for a Manhattan space lattice has an upper bound of 4. This quantity coincides with the Manhattan space infill asymptotic result of a fractal dimension of 2.

Lemma 3. *If $n = 2$, then $\lambda_1 = 2$.*

Proof. Matrix $\mathbf{C} = \begin{pmatrix} 0 & 1 & 1 & 0 \\ 1 & 0 & 0 & 1 \\ 1 & 0 & 0 & 1 \\ 0 & 1 & 1 & 0 \end{pmatrix}$

The sum of each row is 2. By the Perron–Frobinius theorem, $\lambda_1 = 2$. □

Moreover, the smallest fractal dimension for a Manhattan space, which has to be at least 1, coincides with a principal eigenvalue of 2.

3.2. Lattice-Based Fractal Dimension Results

Griffith and Arlinghaus [22] outline the conceptual basis for establishing the fractal dimension of a given n-by-n Manhattan space lattice. The numerical relationship between n and its corresponding fractal dimension, calculated with Fractalyse, may be summarized as follows:

$$\underset{k\to\infty}{limit} \frac{f_{LN}\left[2^{2k}, N\left(2^{k+1}-n\right)\right]}{kLN(2)} \approx 2 - \frac{17.59249}{(n+50.40103)^{0.89149-0.26173\sqrt{n+2.86705}}} \quad (1)$$

where 2^{2k} and $N(2^{k+1} - n)$ are box-counting results, and f_{LN} denotes the presence of a logarithm in the function. The nonlinear least squares estimation of Equation (1), regressing the estimated fractal dimension (i.e., Y) on its corresponding value of n (i.e., X)—based upon the first 25,000 values of n supplemented with every 25,000th one thereafter to 1,000,000, and representing infinity by 10^{32}—has the following diagnostics associated with it (from a nonlinear regression analysis):

Error sum of squares (ESS) = 0.00033 ≈ 0
Relative prediction error sum of squares (PRESS/ESS) = 1.01529
$R^2 > 0.99999 \approx 1$
Bivariate regression coefficients: (intercept) a = 0.00062 ≈ 0, (slope) b = 0.99967 ≈ 1

Equation (1) furnishes an extremely good description of the range of fractal dimensions, from $n = 2$ to $n = \infty$. It approximates the closed form of the logarithm of the N(k) function that is a mixture of 2^{2k} and LN[N($2^{k+1} - n$)] counts. It gives the following out-of-sample estimates of the fractal dimension:

n	Fractal dimension	Equation (1)
45	1.641	1.641
250	1.883	1.881
350	1.911	1.908
500	1.929	1.932
1000	1.934	1.962

These results highlight two features of the analysis. First, Fractalyse is sensitive to the image grayscale and resolution, and consequently has an increasingly challenging task of accurately estimating a dimension as the density of Manhattan space lines increases with increasing asymptotics. Second, the difference for $n = 1000$ (i.e., 1,000,000 vertices on the square lattice grid graph) is rather small, implying that the detected box-counting bias is not excessive.

Because the software is slightly sensitive to grayscale and resolution characteristics, this analysis does not measure the space-filling nature of one-dimensional lines without thickness. However, it appears to measure space-filling by slender, but not truly one-dimensional, line segments. Thus, one should not expect results from the software to exactly match results from direct mathematical calculations based on suitably scaled generators applied to basic patterns to create an infinite hierarchy of form. Nonetheless, because Fractalyse does measure space-filling of lines of varying thickness, it appears to have utility in application where, for example, real-world lines such as roads fill space in a number of ways. Hadzieva et al. [50] assess it and then label it a sufficiently professional, reliable, and consistent software tool to be used for research purposes.

4. Central Place Space: Infill Asymptotics

Arlinghaus [51] shows that scaled hexagonal nets, in one orientation, have Hausdorff–Besicovitch dimension LN(2)/LN($\sqrt{3}$), representing their space-filling character by one-dimensional lines as an infinite process. Different net orientations produce different dimensions. A direct mathematical procedure for a complete characterization of this infinite process, independent of image grayscale or resolution characteristics, appears in her 1985 paper, with a follow-up in Arlinghaus and Arlinghaus [52] of a more detailed proof of method and solutions to existing open questions involving uniqueness. Subsequent works address a variety of related matters, including the use of square nets. Some of these issues appear in the ensuing planning application (see Section 7.2) in this article.

The simplest central place space comprises nine hexagons forming a square region. As for the preceding Manhattan space analysis, central place spaces can be constructed that involve an increasing number of horizontal and vertical sets of points occurring between the landscape defined by these original hexagons. As the number of smaller hexagons approaches infinity, the central place space lattice, as measured in Fractalyse, also converges on a filled-in unit square (Figure 5).

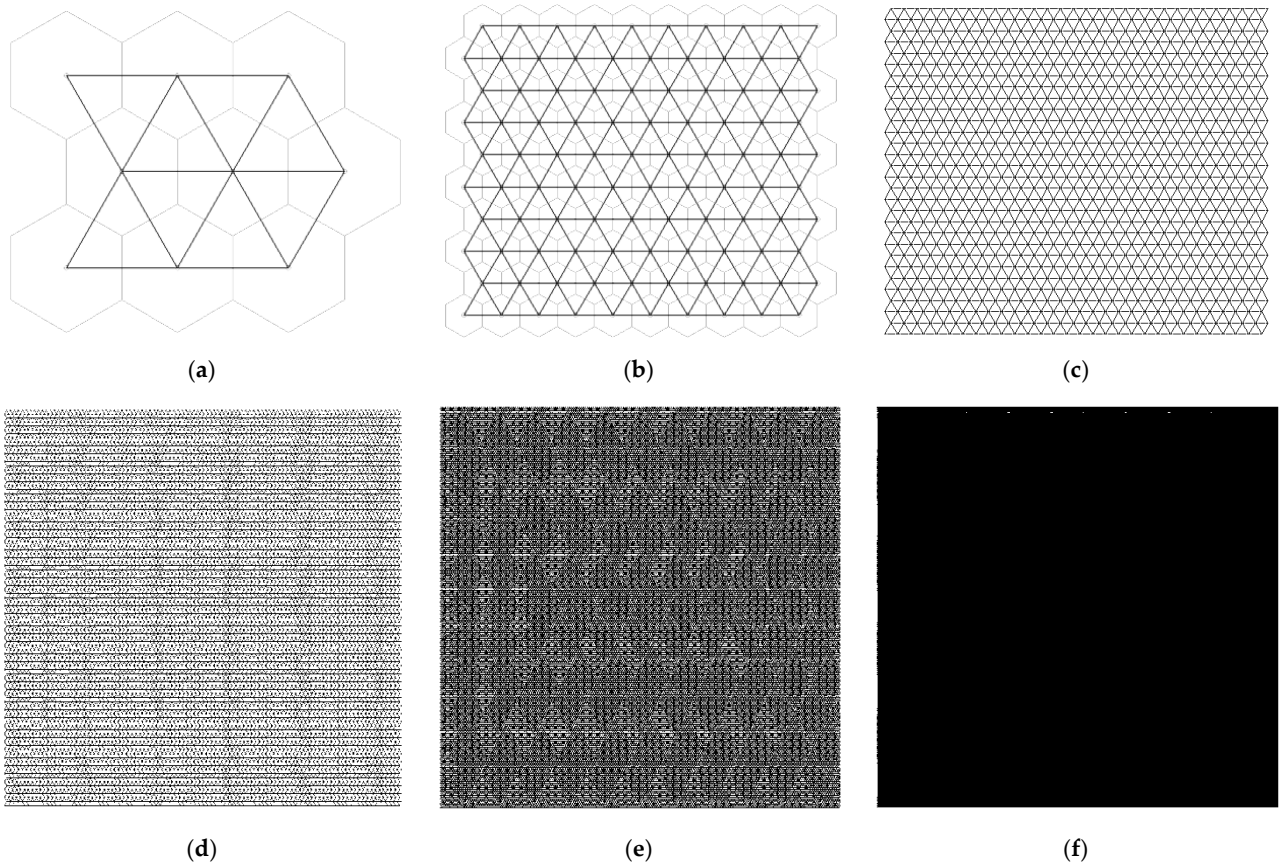

Figure 5. Central place space with increasing n. Top left (**a**): n = 3. Top middle (**b**): n = 10. Top right (**c**): n = 30. Bottom left (**d**): n = 100. Bottom middle (**e**): n = 200. Bottom right (**f**): n = 400.

4.1. Lattice-Based Matrix Algebra Results

This section summarizes an analysis of square-shaped regions of hexagonal tessellations, beginning with a 3-by-3, and ending with a 74-by-74.

Lemma 4. *For a hexagonal lattice,* $\lim_{n\to\infty}\lambda_1 = 6$.

Proof. Each interior node in a hexagonal lattice has six neighbors. As this lattice increases in size to infinity, every row sum of its adjacency matrix becomes 6. By the Perron–Frobinius theorem, $\lambda_1 = 6$. □

Alternatively, mapping the hexagonal grid onto a torus (e.g., [53]), creating a hexagonal mesh toroid, and taking this topological object to an infinite size while preserving the coverage of its individual regular hexagons achieves the same outcome. In other words, the principal eigenvalue of the adjacency matrix, **C**, for a central place space lattice has an upper bound of 6. This coincides with the Manhattan space infill asymptotic result of a fractal dimension of 2.

Griffith [54,55] presents approximation equations for the principal eigenvalue of the 0–1 binary adjacency matrix for the hexagonal lattice. Updates for these equations when the landscape forms a square-shaped region geographic landscape are as follows:

$$\begin{aligned}\hat{r} &= 146.70990\left[1 - 2(84.12680)/(n+164) + 730.66271/(n+14)^2\right]\\ \hat{\lambda}_1(\text{planar}) &= \left\{\left[2(2^r) + n(3^r)2(n-2)(4^r) + (n-2)(5^r) + (n-2)^2(6^r)\right]/n^2\right\}^{1/r}\end{aligned} \tag{2}$$

and

$$\hat{\lambda}_1(\text{torus}) = (1.01812)(4)\left\{COS\left[\frac{\pi}{n+\left(\sqrt{3}\right)/2}\right]\right\} + \left(\frac{3-2(1.01812)}{4}\right)(4)\left\{COS\left[\frac{\pi}{n+\left(\sqrt{3}\right)/2}\right] + COS^2\left[\frac{\pi}{n+\left(\sqrt{3}\right)/2}\right]\right\}. \quad (3)$$

These two approximations enable an extension of the analysis in this section beyond n = 74, a constraint arising from restrictions on PC computer resources needed to calculate the principal eigenvalue. Both approximations converge on 6 in their respective limits

4.2. Lattice-Based Fractal Dimension Results

The numerical relationship between n and its corresponding fractal dimension for a central place landscape, calculated with Fractalyse, may be summarized as

$$\approx 2 - \frac{5.20451}{\left(n+24.16895\right)^{0.73080-0.41160/\sqrt{n+1.67932}}}. \quad (4)$$

This equation is similar to Equation (1) in structure. The nonlinear least squares estimation of Equation (4), regressing the estimated fractal dimension (i.e., Y) on its corresponding value of n (i.e., X)—based upon values of n between 3 and 74 coupled with infinity, represented by 10^{32}—has the following diagnostics associated with it (from a nonlinear regression analysis):

Nonlinear relative error sum of squares (RESS) = 0.00003 $\approx$ 0
Prediction error sum of squares (PRESS)/ESS = 1.28926
R^2 > 0.99999 $\approx$ 1
Bivariate regression coefficients: (intercept) a = 0.00000, (slope) b = 1.00000
Probability (Shapiro–Wilk normality diagnostic for regression residuals) = 0.7318
$\Longrightarrow$ tFail to reject a null hypothesis of normality
The structure of Equations (1) and (4) qualitatively is the same. One difference is that the 4-by-4 graph is the smallest one used to estimate this latter equation (NOTE: the 3-by-3 graph failed to yield consistent fractal dimension estimates; the estimated dimension for n = 3 is 1.127, which better aligns with the other dimension estimates than the value of 1.221 produced by Fractalyse, with other selected out-of-sample predictions being very close to their calculated dimensions by Fractalyse—n = 100, 1.814 versus 1.81352; n = 200, 1.882 versus 1.88376; and, n = 400, 1.917 versus 1.92868).

5. Relationships Between Fractal Dimensions and Principal Eigenvalues of Adjacency Matrices

The preceding sections reveal that a near-perfect correspondence exists between the size of a square or hexagonal lattice, measured in terms of the number of nodes in its graph, n^2, and both its fractal dimension and its principal eigenvalue. These findings imply that a relationship should exist between these two features of a graph too.

5.1. Manhattan Space

The following conjecture posits a relationship between the fractal dimension of Manhattan space and the eigenvalues of a regular square (i.e., planar) lattice:

Conjecture 1. *If a two-dimensional finite Manhattan space forms an n-by-n regular square tessellation on a planar surface, with each of the n^2 points of its associated grid constituting a planar graph node, then the fractal dimension, d, of this space is approximated by*

$$1 - \frac{6.13737}{\left[4.00002^{18.81029} - \lambda_1^{18.81029}(planar)\right]^{1/18.81029}} + 1995\frac{\left[\lambda_1^{2.202570} - \lambda_1^{2.20257}(planar)\right]^{1/2.20257}}{n^{1.64332}+19468} + \frac{6.13737}{\left(4.00002^{18.81029} - \lambda_1^{18.81029}\right)^{1/18.81029}}, \quad (5)$$

where λ_1 is from Lemma 1, its asymptotic value of 4 is from Lemma 2, and $\lambda_1(planar) = 2COS\left[\pi / \left(n^2+1\right)\right]$, the principal eigenvalue for a line graph with n^2 nodes.

Evidence 1. *Figure 6 presents scatterplots affiliated with Equation (5). Figure 6a portrays the overlay of the relationships between the fractal dimension and λ_1, and the predicted fractal dimension and λ_1. Figure 6b portrays the relationship between the box-counting fractal dimension determined by Fractalyse and the fractal dimension predicted by Equation (5). In addition (from a nonlinear regression analysis):*

Nonlinear relative ESS (RESS) = 0.00077 ≈ 0
Relative prediction error sum of squares (PRESS/ESS) = 1.04456
Pseudo-R^2 = 0.9992 ≈ 1
Bivariate regression coefficients: (intercept) a = 0.00163 ≈ 0, (slope) b = 0.99909 ≈ 1
The graphical depiction of Equation (5) resembles a left-truncated sinusoidal random variable distribution, which the powered difference entry in the denominator of its first and third terms reflects.

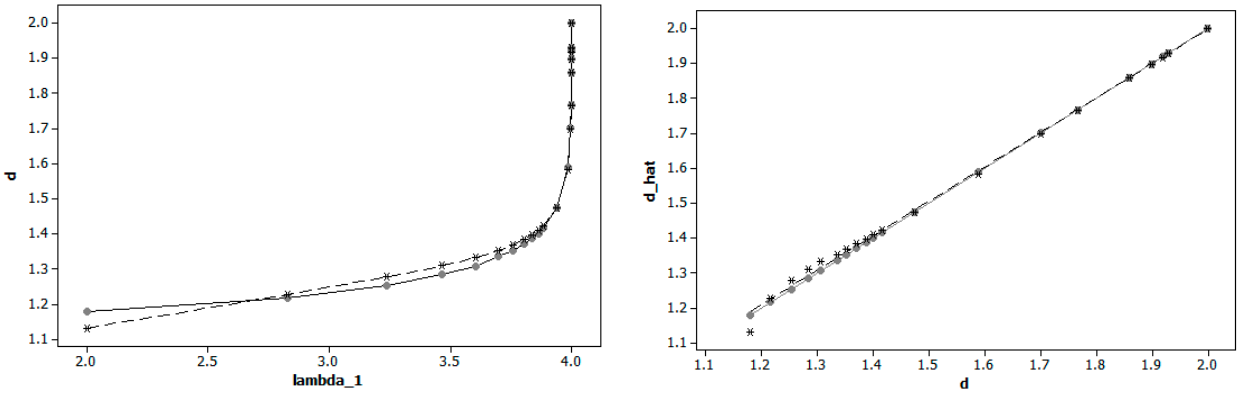

(**a**) (**b**)

Figure 6. Respectively, black asterisks and dashed lines denote predicted values, and gray solid circles and solid lines denote observed values. Left (**a**): Equation (5) overlay scatterplots for observed and predicted fractal dimensions versus principal eigenvalues for Manhattan spaces. Right (**b**): scatterplot of fractal dimensions versus Equation (5) predicted values.

Equation (5) has two noteworthy properties. First, regardless of the size of a line graph, its calculation yields the correct dimension of 1. Second, its asymptotic dimension is constrained to be 2 for $\lambda_1 = 4$ (Lemma 2).

The principal implications here are as follows:

(1) As *n* increases, the delineated space converges on a bounded Euclidean plane by becoming increasingly filled; and,
(2) The finite Manhattan space fractal dimension relates to the corresponding regular lattice planar graph principal eigenfunction.

One higher-order implication is that an undeniable bond exists between fractals and spatial autocorrelation (e.g., [56]).

5.2. Central Place Space

The following conjecture posits a relationship between the fractal dimension of central place space (e.g., see [57,58]) and the eigenvalues of a regular hexagonal lattice:

Conjecture 2. *If a two-dimensional finite central place space forms an n-by-n planar regular hexagonal tessellation, with each of the n^2 points of its associated grid constituting a planar graph node, then the fractal dimension, d, of this space is approximated by*

$$1 - \frac{12.26546}{\left[6.00015^{19.17466} - \lambda_1^{19.17466}(planar)\right]^{1/19.17466}} + 1004\frac{\left[\lambda_1^{0.36328} - \lambda_1^{0.36328}(planar)\right]^{1/0.36328}}{n^{1.22959}+681} + \frac{12.26546}{\left(6.00015^{19.17466} - \lambda_1^{19.174666}\right)^{1/19.17466}}, \quad (6)$$

where the asymptotic value of 6 for λ_1 is from Lemma 4, λ_1 is the average of Equations (2) and (3) for values of $n > 74$, and $\lambda_1(planar) = 2COS\left[\pi / \left(n^2+1\right)\right]$.

Evidence 2. *Figure 7 presents scatterplots affiliated with Equation (6). Figure 7a portrays the overlay of the relationships between the fractal dimension and λ_1, and the predicted fractal dimension and λ_1. Figure 7b portrays the relationship between the box-counting fractal dimension determined by Fractalyse and the fractal dimension predicted by equation (6). In addition (from a nonlinear regression analysis):*

Nonlinear RESS = 0.00000
Relative prediction error sum of squares (PRESS/ESS) = 1.03186
Pseudo-R^2 = 0.99999 ≈ 1
Bivariate regression coefficients: (intercept) a = 0.00080 ≈ 0, (slope) b = 0.99956 ≈ 1
The graphical depiction of Equation (6) also resembles a left-truncated sinusoidal random variable distribution.

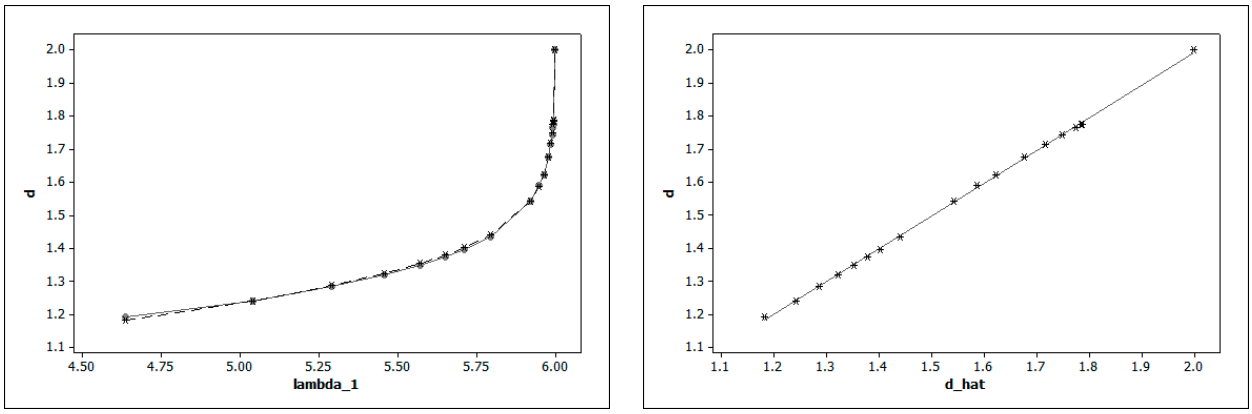

(**a**) (**b**)

Figure 7. Respectively, black asterisks and the dashed line denote predicted values, and gray solid circles and solid lines denote observed values. Left (**a**): Equation (6) overlay scatterplots for observed and predicted fractal dimensions versus principal eigenvalues for central place spaces. Right (**b**): scatterplot of fractal dimensions versus Equation (6) predicted values.

Equation (6) also has two noteworthy properties. First, regardless of the size of a line graph, its calculation yields the correct dimension of 1. Second, its asymptotic dimension is constrained to be 2 for $\lambda_1 = 6$ (Lemma 4).

Therefore, the principal implications for central place geometry derived here parallel those for Manhattan space.

5.3. Dual Planar Graphs for Irregular Surface Partitionings

Equations (5) and (6) are constrained such that their asymptotic principal eigenvalues coincide with a filled square's fractal dimension of 2. But many graphs, especially ones without a pattern, do not have a known maximum principal eigenvalue; even some patterned graphs have infinite extreme eigenvalues [59]. The following conjecture posits a relationship between the fractal dimension of these unpatterned graphs and the eigenvalues of their dual planar networks based upon 23 conveniently available but arbitrary empirical and ideal planar graphs selected to cover a reasonable range of principal eigenvalues (example networks appear in Figure 8):

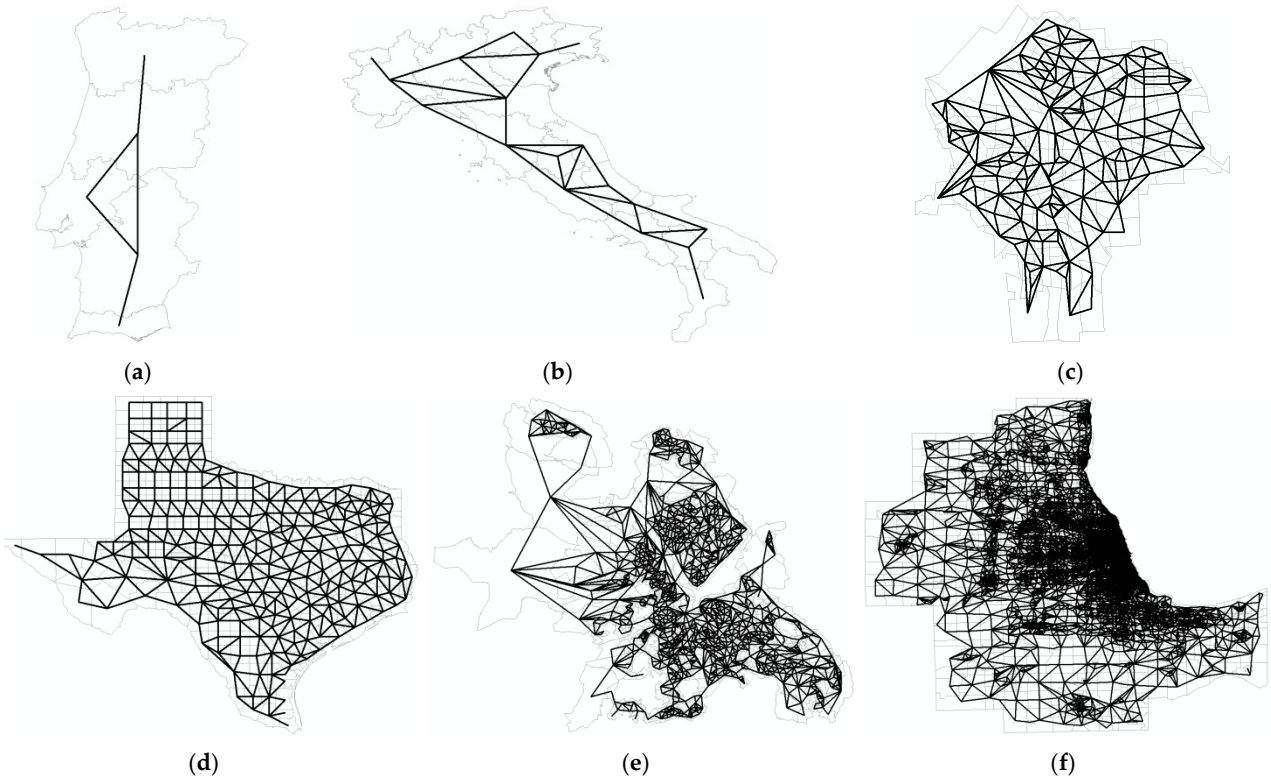

Figure 8. Dual graphs based upon centroid points (their counts denoted by P) from irregular surface partitionings. Top left (**a**): Portugal NUTS-2 (P = 5). Top middle (**b**): Italy NUTS-2 (P = 18). Top right (**c**): Syracuse US census block groups (P = 146). Bottom left (**d**): Texas counties (P = 254). Bottom middle (**e**): Sheffield UK enumeration districts (P = 930). Bottom right (**f**): Chicago US census block groups (P = 6628).

Conjecture 3. *If a two-dimensional finite surface is partitioned into n mutually exclusive and collectively exhaustive irregular polygons, with the centroid of each polygon constituting a node of a planar graph, then the fractal dimension, d, of this network is approximated by*

$$1 - \frac{242}{\left[\lambda_n^{17.54513}(max)+1.46498\right)^{8.97926}-\lambda_n^{8.9792}(planar)]^{1/8.9792}} + \frac{2}{\lambda_n(planar)+\ 6.48816/n^{0.41957}} + \frac{242}{\left[\lambda_n^{17.54513}(planar)+1.46498\right)^{8.97926}-\lambda_1^{8.9792}]^{1/8.9792}} - \frac{2}{\lambda_1+\ 6.48816/nP^{0.41957}}, \quad (7)$$

where $\lambda_n(planar) = 2COS[\ \pi\ /(n+1)]$ *for a line graph, and*

$$\lambda_n(max) = \{1 + 2COS[\pi\ /(n-1)]\}/2 + \sqrt{2n - \{13 + 4COS[\pi/(n-1)] - 2COS[2\pi/(n-1)]\}/4}$$

for the maximum connectivity planar case [59].

Evidence 3. *Figure 9 presents scatterplots affiliated with Equation (7). Figure 9a portrays the overlay of the relationships between the fractal dimension and λ_1, and the predicted fractal dimension and λ_1. Figure 9b portrays the relationship between the box-counting fractal dimension determined by Fractalyse and the fractal dimension predicted by Equation (7). In addition:*

Nonlinear relative ESS (RESS) = 0.00105
Relative prediction error sum of squares (PRESS/ESS) = 1.15904
Pseudo-R^2 = 0.9518
Bivariate regression coefficients: (intercept) a = 0.05339, (slope) b = 0.96194

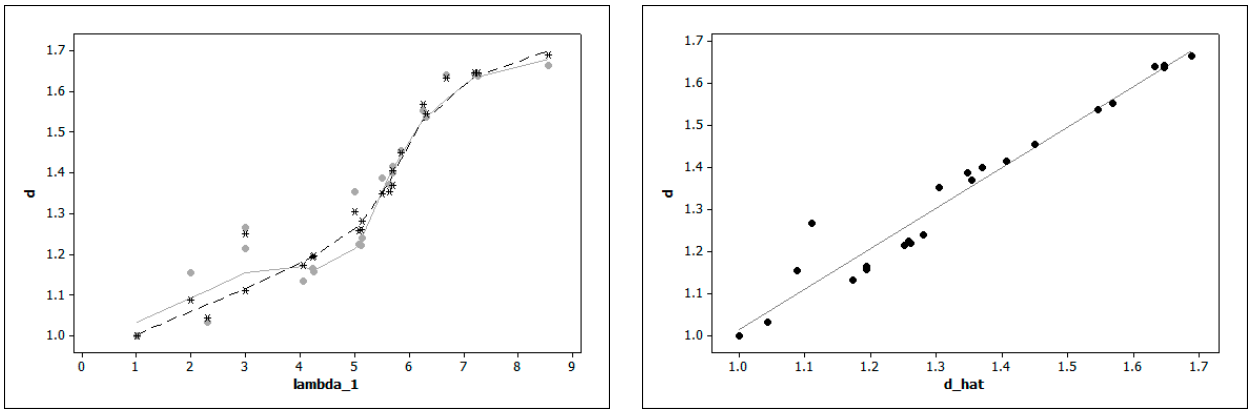

(**a**) (**b**)

Figure 9. Respectively, black asterisks and the dashed line denote predicted values, and gray solid circles and solid lines denote observed values. Left (**a**): Equation (7) overlay scatterplots for observed and predicted fractal dimensions versus principal eigenvalues for central place spaces. Right (**b**): scatterplot of fractal dimensions versus Equation (7) predicted values.

For a straight line with two or more nodes (i.e., a line graph), Equation (7) equals 1; for an infinite triangular graph (see [60]), Equation (7) equals 2. In contrast to Equations (5) and (6), the graphical depiction of Equation (7) resembles a logistic-type S-shaped curve. Its description is poorer than those for the other two geometries because the specimen graph links vary in length and lack a global pattern. Potentially, more evidence for this case might be gleaned from studies of two-dimensional Thiessen polygon (also known as Voronoi diagram cells) surface partitionings.

6. Selected Relationships Between the Fractal Dimension Concept and Spatial Statistics

This foregoing principal eigenfunction of a planar graph represents the geographic distribution of network accessibility across its set of nodes (e.g., [61,62]). In keeping with this notion, Equation (5) relates Manhattan space and spatial statistics, consistent with relationships between fractal networks and both graph theory and combinatorics [63]. The network structure meaning of the principal eigenvector of a planar graph is a location-by-location index of accessibility based upon all possible topological ways of moving between a pair of nodes traversing exactly h links: $\sum_{h=0}^{D} \mathbf{C}^h$, where **C** is the binary 0–1 adjacency matrix and D is the diameter of a network (graph). This eigenvector is known analytically [54] to be $\mathbf{E}_1$ in which element $eij1 = \frac{2}{n+1} SIN\left(\frac{i\,\pi}{n+1}\right) SIN\left(\frac{j\,\pi}{n+1}\right)$, i = 1, 2, . . ., *n* and j = 1, 2, . . ., *n* for a regular square lattice graph. Figure 10 furnishes selected geographic mappings of this eigenvector. All six of these maps indicate that the center of a given Manhattan space has the highest degree of accessibility and that the periphery of this space has the lowest.

This accessibility index has a concentric circle decline with increasing distance from the center of the unit square. As Manhattan space becomes increasingly dense through infill asymptotics, its Euclidean counterpart increasingly reflects this same property.

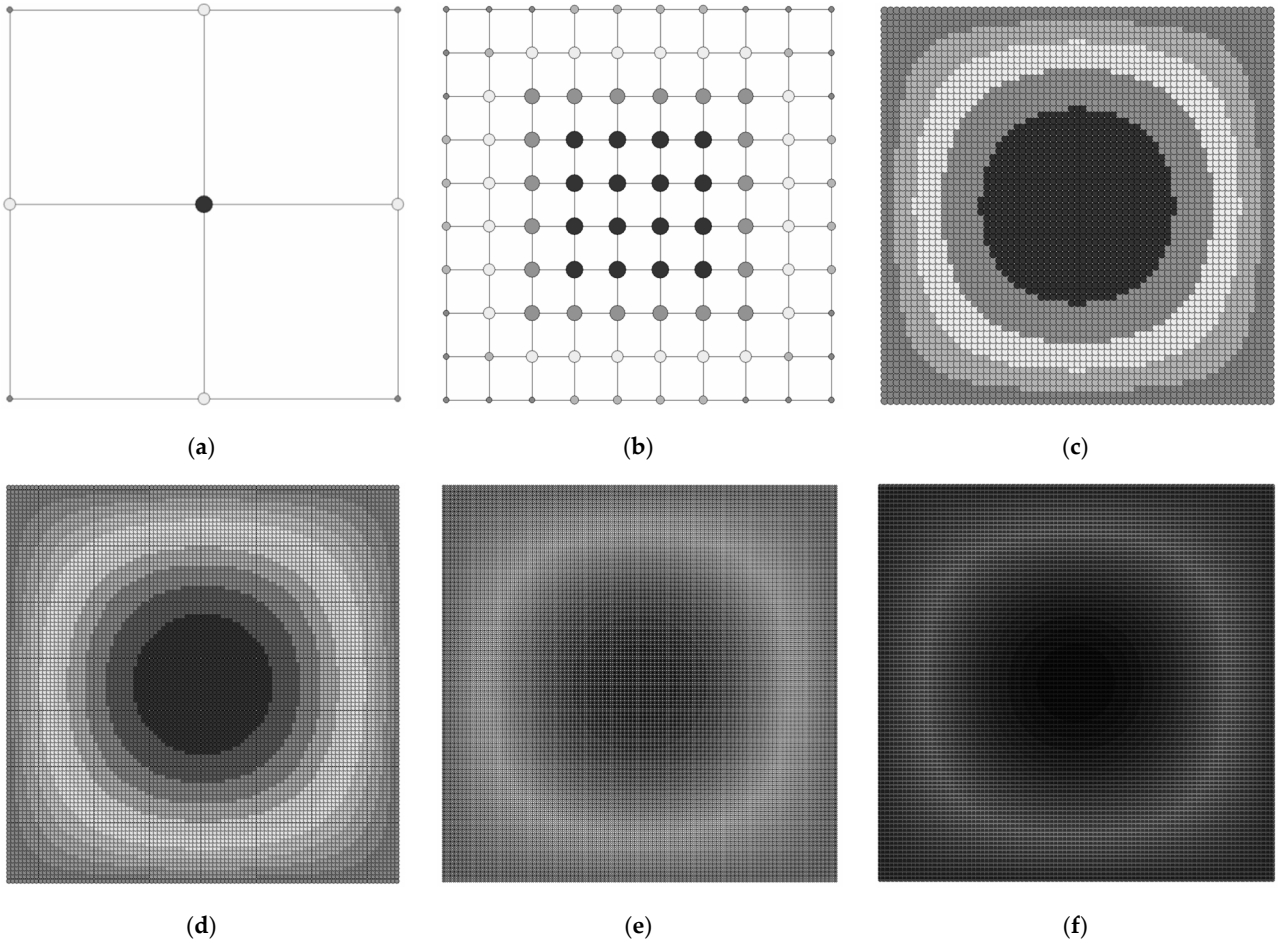

Figure 10. Geographic distribution of the principal eigenvector for Manhattan space with increasing values of P, where P^2 is the number of points; accessibility is directly proportional to the darkness of the grayscale. Top left (**a**): P = 3. Top middle (**b**): P = 10. Top right (**c**): P = 33. Bottom left (**d**): P = 99. Bottom middle (**e**): P = 197. Bottom right (**f**): P = 400.

Maps similar to those appearing in Figure 10 can be constructed for Equations (6) and (7).

7. Concentric Circles, Grids, Fractally-Bound Pattern Compression, and Urban Planning

The preceding discussion addresses selected mathematical properties of planar graph fractal dimensions, explicitly referencing non-Euclidean geometries, with an aim of furnishing a context for empirical and numerical applications. It includes an example of Chicago (Figure 8f), based upon 2000 census block group areal units. This section extends this Chicago focus as it tackles a particular fractal application involving real-world as well as abstract map images.

7.1. A Classical Chicago Urban Setting

Although models themselves are abstract and artificial, they often serve as powerful tools for visualizing and clarifying complex issues in real-world contexts. Simple formulations, in particular, can offer significant insight. One such model, developed in the early 20th century, is the Burgess description of urban spatial structure, which initially was ap-

plied to Chicago. Its concentric ring pattern remains a useful starting point for investigating urban road networks today. In particular, it provides a foundation for analyzing street patterns using more modern tools, such as Fractalyse.

In the third decade of the last century, mapping Chicago's road network alongside the Park and Burgess [64] concentric ring zones would have been a daunting task. However, with today's advanced technology, this task is relatively straightforward. This execution parsimony is specifically exemplified in the work of Arlinghaus and Griffith [65], who overlay the Burgess rings on a map of Chicago's modern road network using Google Earth. Their process requires several technical steps, including aligning the historical street patterns of the 1920s with the city's current infrastructure. To do this, these authors used a map titled "Chicago's Gangland" [66], which is available online through the University of Chicago Library. This map, though useful, has an unknown projection, so these two researchers employed a piecewise strategy, similar to creating a globe from multiple segments, to fit the map's features to the Google Earth globe.

Visualizing the combined map of Chicago's road network and the Burgess rings requires digital tools like Google Earth, which are not available in a printed format. Nevertheless, a full interpretation of the street patterns within the rings is still challenging. Fortunately, by mapping the city's street data using Tiger Line files from the United States Census Bureau and then overlaying it with the Burgess rings, this visualization becomes clearer. The Arlinghaus and Griffith [65] analysis shows how GIS software can be used to map such street patterns, producing a layered image that reveals distinct layouts.

Figure 11 presents the Burgess rings superimposed on a GIS map of Chicago's streets. This image reveals open spaces, such as river valleys, expressways, and parks, as well as a decrease in street density as one moves outward from the city center. Circular spatial samples in the image highlight typical street patterns within each ring, allowing for a closer examination of the existing road network. Using Fractalyse, the two authors of this earlier paper calculated numerical measures of street density within each ring, confirming the visual observation that street density diminishes as one moves further from the center.

One reason for undertaking such an analysis is to develop a strategy to measure phenomena in the otherwise onerous and uncontrollable laboratory of the real world. Another is to make measurement replication coherent across different urban areas. Meanwhile, factors other than mere projected street density may be of interest as well. Although such street pattern density might be of interest in planning applications that must consider parking situations surrounding a large venue, such as a baseball park or big apartment building, its extent also might be critical in transportation planning applications that need to consider routing alternatives as well as physical access to the target population to be served. This paper additionally illustrates that a strategy similar to that employed for measuring density also works for magnitude.

In order to assess space-filling degree, the Fractalyse box-counting method was used to create a numerical measure of each of the four bounded areas (Figure 11 zone E is unbounded) in the set of concentric zones in the Burgess-rings-superimposed-upon-streets visualization. With scale held constant, moving in a direction away from the city center, the space-filling values of the four bounded rings increase in the following manner: 1.25, 1.466, 1.496, and 1.593 (Figure 12). This numerical pattern appears because more of the analysis box is filled with lines by the larger regions. If one zooms in to fill the analysis box, then the scale is altered and no longer held constant. Consistent areal sampling can overcome such difficulties, although such sampling certainly has issues of its own.

Figure 11. Region A, many alleys separate blocks: dim = 1.284. Region B, a few alleys: dim = 1.258. Region C, blocks, a bit larger: dim = 1.209. Region D, blocks, a bit larger, along with more open space: dim = 1.198. Region E, irregular patterns not uncommon with open space: dim = 1.181.

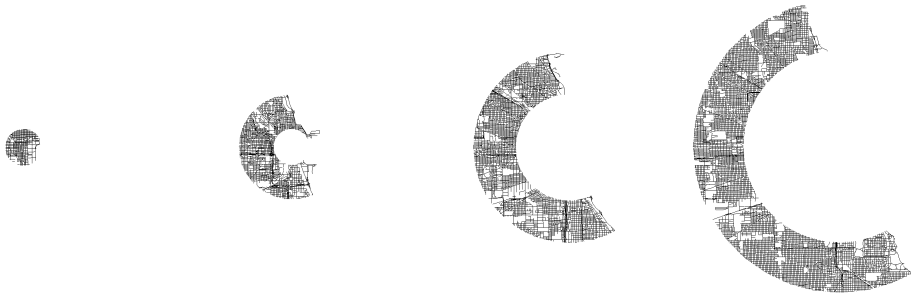

(**a**) (**b**) (**c**) (**d**)

Figure 12. Disassembly of four interior rings of the Park–Burgess [64] model into components and associated space-filling dimensions. The dimension increases as the pattern enlarges in coverage: from left to right, (**a**) 1.25 → (**b**) 1.466 → (**c**) 1.496 → (**d**) 1.593. Here, the extent, rather than the density, of the pattern is being measured.

One might conjecture that because the concentric circles/rings of the Burgess graphical model reflect different land use densities, they should contain different underlying road pattern densities. The application of a single fractal iteration sequence would not generate an appropriate pattern, or its compression. The preceding analysis furnishes solid support for these ideas. In contrast, the next sections consider how to employ multiple fractal-style analyses to create urban form, and then from there, how to move back again to the abstract world of eigenvalues. Rather than offering a rigid set of predetermined rules, the sections' narratives reflect upon these actions as they develop so that the gained flexibility offers a possibility for application in multiple, perhaps unforeseen, arenas.

7.2. Fractally Bounded Planning

Empirical evidence from Chicago, using the Burgess model, implies the appropriateness of calibrating networks to different fractal dimensions depending upon land use

types. This idea, coupled with that of truncating a fractal iteration sequence based upon desired parcel size, as in a marina example [67], offers a clear way to build urban networks. The first step is possibly defining an advanced determination of the permitted extent of space-filling by a road network as a new class of zoning. Traditional parcel code usage regulations primarily decree such filling by buildings and land use types. A second step is to employ the proper fractal dimensions, generated as absolute (rather than as relative) values based upon an iteration of self-similar generators applied to an initiator. Fractal generation of this geometric sort is independent of resolution and various other issues that cloud the utility of otherwise reputable software such as Fractalyse.

With regard to a practical implication, Arlinghaus [51] first portrayed the utility of employing geometric generation, based upon a hexagonal pattern, to characterize all possible classical central place webs, using that approach to solve previously unsolved classical Christaller central place theory problems. This solution relies on creating geometric generators to be applied iteratively and then employing the Hausdorff–Besicovitch dimension calculations to capture the space-filling character of central place nettings centered on hierarchies of metropolitan areas, cities, towns, and villages. Later, in 1989, Arlinghaus and Arlinghaus [68] presented the details of number-theoretic components supporting these geometric constructions. In 1991, Arlinghaus [57] adjusted this sequential process applied to hexagons to work with squares, in keeping with urban road networks perhaps more than hexagons do. This revision exemplifies an instance in which letting the possibly irregular demands of the uncontrolled real-world laboratory dictate which abstract tool to employ, rather than the reverse, is important in a practical situation: the best practice is to account for problems before an analysis, rather than trying to explain multiple outliers after the analysis.

This category of idea is similar to urban downtown planning: fill an area with buildings as allowed by zoning, and put in as many roads as possible to facilitate movement; superimpose a park if desired, but as an overlay on the fundamental strategy; and use the value of $d = 2$ as the upper bound beyond which space-filling by roads is not permitted. Employing a maximum value allows looser space-filling within a region outside its central area, corresponding in the real world, perhaps, to many patterns of typical suburban residential developments. These constructions are complex in visual appearance and are perhaps best realized in color; a summary of a number of such approaches, along with associated extensions of number theory connections, is visualized in interactive models in Arlinghaus and Arlinghaus [68].

In their 2014 work, Arlinghaus and Griffith [69] suggest extending the Burgess model by adding more concentric rings, potentially reflecting different residential zoning types. Their approach involves introducing traffic circles or rotaries at ring boundaries, depending upon the type of fractal pattern used to fill the zones. As one moves from one ring to another, cul-de-sacs also appear, forming enclaves that could be linked to specific zoning patterns. The process for creating these patterns begins by generating a fractal road grid, which is then modified according to parcel size based upon statute land use and zoning regulations.

Aligning the patterns at the boundaries of adjacent rings can be challenging, because road networks from neighboring rings may not match perfectly due to differences in iteration sequences used to fill space. One solution could involve aligning the core road network boundary points and inserting traffic circles where appropriate. Any remaining points could become cul-de-sacs, which might be beneficial for residential areas seeking privacy or for industrial areas that want a lower profile. In this approach, cul-de-sacs serve a functional purpose—acting as a vestigial element in an otherwise efficient road network, unlike in traditional urban planning where their use is often questioned.

The varying spatial needs of different zoning categories create distinct neighborhoods within a road network. This structure promotes easy accessibility within each ring while

limiting access between rings, potentially enhancing safety. It also may add visual interest to an otherwise monotonous grid pattern. Of course, the urban model, zoning strategy, and/or planning context can be adjusted to suit specific needs, but fractally bounded plans can serve as a useful guide in real-world urban planning.

7.3. Eigenvalues and the Direct Mathematical Generation of Fractals

One way to calculate the Hausdorff–Besicovitch dimension is through the use of a generator applied at successive scales, building upon some initial shape. This process involves repeatedly applying this generator to create new self-similar shapes, forming an infinite sequence that converges to a finite value. Selecting the generator is a nuanced task. While the scaling effect is clear, the role of eigenfunctions (i.e., eigenvectors and eigenvalues) remains subtle, often only implicitly present in a generator's geometry.

Arlinghaus [57] demonstrates this method using a K = 7 Christaller central place model, illustrating how eigenvalues emerge in the process. She generates a fractal sequence using a single shape, a 4-star graph, that slides across a geographic landscape using vectors to create a repeating pattern. Figure 13 depicts this process: starting with a four-star shape (Figure 13a), a vector is applied to shift it to the right (Figure 13b), with this transformation repeating (Figure 13c); next, a vector orthogonal to the first one is applied to shift this four-star shape in a different direction (Figure 13d), continuing the transformation (Figure 13e); finally, both vectors are used to fill the remaining space (Figure 13f). The eigenvectors create a fractal pattern, with the corresponding eigenvalues determining how much these eigenvectors are stretched or compressed. If each eigenvector has a unit length (i.e., 1), the other eigenvalues are positive and negative integers. If this geometric form is overlaid on a coordinate system, the eigenvalues may be integral multiples of the basic value. Figure 13 shows where these eigenvectors are lurking in this process, as they correspond to the edges of the polygon onto which the generator is applied.

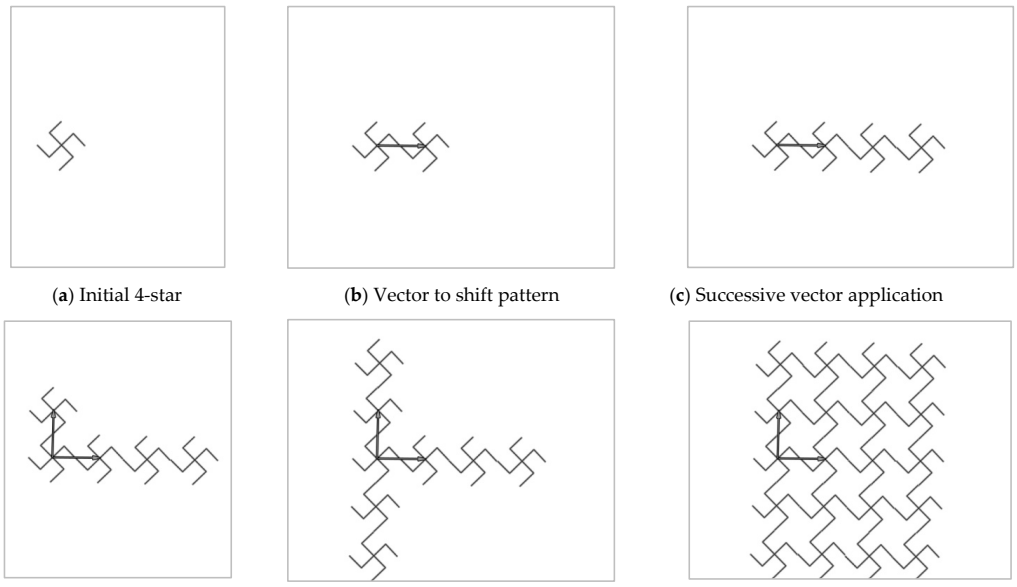

(**a**) Initial 4-star (**b**) Vector to shift pattern (**c**) Successive vector application

(**d**) Vertical shift (**e**) Successive vertical vector application (**f**) Using the pair of vectors to fill in the pattern

Figure 13. Use of a 4-star shape to generate a pattern identical to that portrayed in Arlinghaus [57]. Here, however, a horizontal vector stretches to slide this 4-star graphic across the plane, and then a vertical vector performs an equivalent transformation to fill space with 4-stars in positions that create the required pattern. These vectors function as two sets of eigenvectors with eigenvalues corresponding to the stretching of the vectors required to create the appropriate pattern.

The sequence appearing in Figure 13 illustrates the first layer of the pattern under study. To generate additional layers, consider a single teragon (Figure 14a). Begin by introducing the four-star graph again (Figure 14b). Apply a vector to transform it (Figure 14c) and then repeat this transformation in the same direction (Figure 14d). Next, apply an orthogonal vector to shift the graph (Figure 14e) and continue applying this transformation in both directions (Figure 14f).

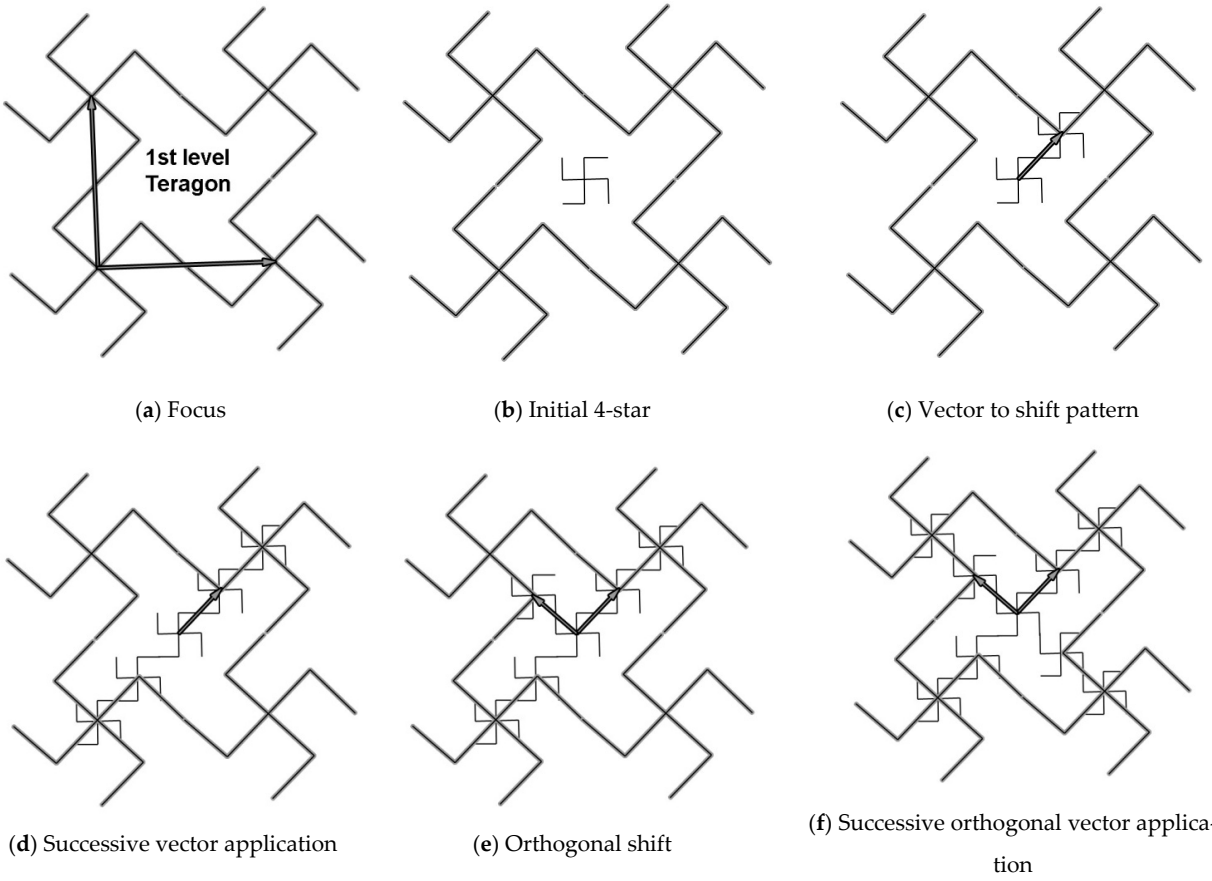

(**a**) Focus (**b**) Initial 4-star (**c**) Vector to shift pattern

(**d**) Successive vector application (**e**) Orthogonal shift (**f**) Successive orthogonal vector application

Figure 14. Use of a 4-star shape to generate pattern identical to that in Arlinghaus [57]. Here, however, one vector stretches to slide this 4-star graphic across the plane, and then an orthogonal vector performs an equivalent transformation to fill space with 4-stars in positions that create the required pattern. These vectors function as two sets of eigenvectors with eigenvalues corresponding to the stretching of the vectors required to create appropriate pattern.

Combinations of the vectors in Figure 14 expand pattern to fill space. Figure 15a portrays this space-filling process together with the pattern of basic vectors in relation to each other: both orientation and length. Figure 15b shows that the process creates eight scaled-down teragons similar to their initial one (e.g., Figure 14a), as required for the construction to possess fractal-based self-similarity. Once again, the positions of the vectors, in relation to the boundaries of polygons appearing in Arlinghaus [57]—i.e., a Christaller K = 4 style of central place hierarchy—show where these eigenvectors are located within the underlying geometry.

The previously displayed construction sequences, suggesting infinite processes, lead to the same results. A crucial difference is that the role of eigenvectors and their accompanying eigenvalues is hidden in the background in the first, while it is displayed in the second, creation. A focus on a planning application, and a need to look for a systematic description of that application, lead back to the theoretical realm for an explanation about how geometry and linear algebra are linked.

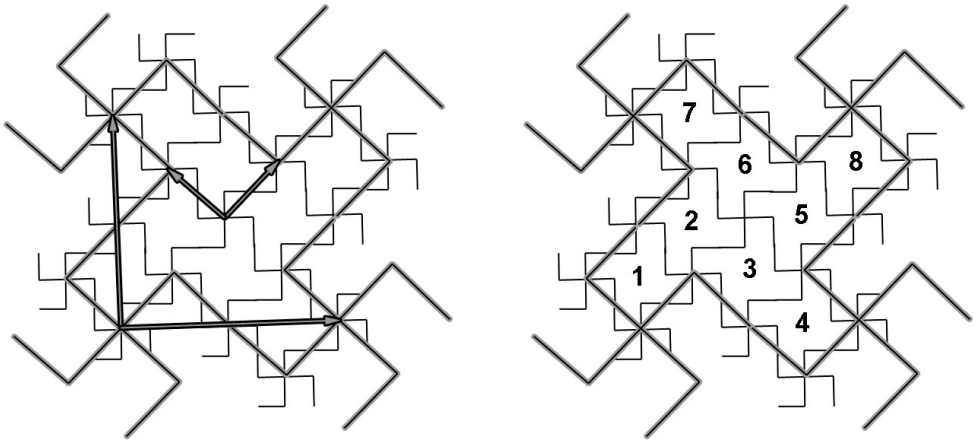

(**a**) (**b**)

Figure 15. The space-filling process continued; the numbers 1–8 label the eight self-similar regions in the graphic. Left (**a**): Output from a set of two orthogonal eigenvectors used to generate each layer of pattern. Right (**b**): The required eight labeled self-similar regions, suggesting a method for continuing the infinite process using 4-star graphs.

8. Discussion, Conclusions, Implications, and Future Research

In conclusion, this paper offers both theoretical and practical contributions to the fields of urban spatial structure and fractality (e.g., [70,71]). It provides an overview of empirical findings regarding a relationship between the non-Euclidean geometry of Manhattan space and fractals, expanding on existing discussions in the literature, some of which pertain to more general Minkowski spaces. This paper also includes enough technical detail to enable readers with a keen interest in its content to replicate and build upon the outlined work.

The empirical analysis this paper exploits focuses on minimum path metrics that describe distances between locations in non-Euclidean urban spaces. A general Minkowski metric, with exponents between those of Manhattan space (exponent of one) and Euclidean space (exponent of two), best represents these distances. Minkowski geometry [72] is most suitable here because it is the domain of normed real finite dimensional vector spaces, one with an appealing connection to differential geometry, as well as an invaluable precursor to the development of Finsler geometry (i.e., a branch of differential geometry that generalizes Riemannian geometry by allowing interpoint distances to depend not only on their relative locations but also on a direction between them). The results from the more general Minkowski metric also relate to the fractal dimensions of the physical spaces involved. A key takeaway from this inquiry is that both theoretical and applied ideas based upon fractals and the Manhattan distance metric are valuable when developing or refining mathematical spatial theories.

Finally, as highlighted by Arlinghaus and Griffith [65], the classical Burgess (concentric ring) model of urban spatial structure presents a promising foundation for incorporating fractal elements into city street networks. Cells in a street pattern conceptually correspond to abstract cells in analytic procedures. These two authors detail the mechanics of this reformulation using fractal geometry and suggest potential applications in urban planning. While these ideas open exciting new avenues for exploration, much more research is needed to fully understand the connection between urban spatial structure and fractality, a topic that already has been under investigation for nearly four decades (e.g., [73]).

In closing, this paper alludes to various potentially fruitful future research endeavors. For example, the purposeful samples of abstract and empirical network specimens studied here and elsewhere warrant a reliability-of-findings assessment of their statistical significance (i.e., sampling error, given drawing a bona fide random sample of networks is

impractical/infeasible), uncertainty components, and error corruptions (e.g., measurement, computational/numerical, specification, and stochastic). Meanwhile, in keeping with the notion of measurement error concerns, because four different fractal dimension calculation methods exist—grid/box-counting, dilation, radial, and correlation (e.g., see [50])—a comparative replication of this study most likely would be illuminating, particularly because the literature, especially studies focusing on street-based approaches, often resorts to the correlation implementation. A third conspicuous future research theme, one underscoring replicability, is a comparative analysis across a set of cities other than Chicago (the Burgess model birthplace) and conceptualizations devised in terms of the Hoyt sector and/or the Harris and Ulmann multiple nuclei urban spatial structure models. A fourth possibility derives from the future tendency of more people working from home, and hence receiving more direct deliveries of food and other consumer items customarily purchased on their journey home from work: the scalability of urban surface networks will need to match, or at least accommodate, these new changes in behavioral patterns across urban street networks that may become non-Euclidean in various ways. Fractals pose an ideal means to scale responses to such changing trends. Of course, one can glean other research themes from this article.

Author Contributions: Conceptualization, S.L.A. and D.A.G.; methodology, S.L.A. and D.A.G.; software, S.L.A. and D.A.G.; validation, S.L.A. and D.A.G.; formal analysis, S.L.A. and D.A.G.; investigation, S.L.A. and D.A.G.; resources, S.L.A. and D.A.G.; data curation, S.L.A. and D.A.G.; writing—original draft preparation, S.L.A. and D.A.G.; writing—review and editing, S.L.A. and D.A.G.; visualization, S.L.A. and D.A.G.; supervision, S.L.A. and D.A.G.; project administration, S.L.A. and D.A.G. All authors have read and agreed to the published version of the manuscript.

Funding: This research received no external funding.

Data Availability Statement: Most data can be self-generated or retrieved from accessible public sources. Certain data are available by making a reasonable data request to the authors.

Conflicts of Interest: The authors declare no conflicts of interest.

References

1. Mandelbrot, B. *The Fractal Geometry of Nature*; Freeman: New York, NY, USA, 1983.
2. Elert, G. Chapter 3: About dimension (3.3 Fractal Dimension). The Chaos Hypertextbook: Mathematics in the Age of the Computer; 1998–2016. Available online: http://hypertextbook.com/chaos/33.shtml (accessed on 28 November 2024).
3. Benguigui, L.; Daoud, M. Is the suburban railway system a fractal? *Geogr. Anal.* **1991**, *23*, 362–368. [CrossRef]
4. Puente, C.; Castillo, P. On the fractal structure of networks and dividers within a watershed. *J. Hydrol.* **1996**, *187*, 173–181. [CrossRef]
5. Shen, G. A fractal dimension analysis of urban transportation networks. *Geogr. Environ. Model.* **1997**, *1*, 221–236.
6. Long, G.; Cai, X. The fractal dimensions of complex networks. *Chin. Phys. Lett.* **2009**, *26*, 088901. [CrossRef]
7. Rosenberg, E. *A Survey of Fractal Dimensions of Networks*; Springer: Cham, Switzerland, 2018.
8. Rosenberg, E. *Fractal Dimensions of Networks*; Springer: Cham, Switzerland, 2020; Volume 1.
9. Wen, T.; Cheong, K. The fractal dimension of complex networks: A review. *Inf. Fusion* **2021**, *73*, 87–102. [CrossRef]
10. Dong, S.; Yu, X.; Zeng, L.; Ye, J.; Wang, L.; Ji, C.; Fu, K.; Wang, R. Relationship between box-counting fractal dimension and properties of fracture networks. *Unconv. Resour.* **2024**, *4*, 100068. [CrossRef]
11. Rashid, M. *The Geometry of Urban Layouts*; Springer: Cham, Switzerland, 2017.
12. Long, Y.; Chen, Y. Multifractal scaling analyses of urban street network structure: The cases of twelve megacities in China. *PLoS ONE* **2021**, *16*, e0246925. Available online: https://journals.plos.org/plosone/article?id=10.1371/journal.pone.0246925 (accessed on 12 January 2025). [CrossRef] [PubMed]
13. Yang, Y.; Fu, B. Spatial heterogeneity of urban road network fractal characteristics and influencing factors. *Sustainability* **2023**, *15*, 12141. Available online: https://www.mdpi.com/2071-1050/15/16/12141 (accessed on 12 January 2025). [CrossRef]
14. Omali, T. Fractal geometry and its application in geographic information science. *Int. J. Sci. Res. Multidiscip. Stud.* **2023**, *9*, 116–120. Available online: https://www.isroset.org/pdf_paper_view.php?paper_id=3336&12-ISROSET-IJSRMS-09261.pdf (accessed on 12 January 2025).

15. Badiei, N.; Almodaresi, S.; Saraei, M. A systematic review of fractal theory and its application in geography and urban planning. *Int. J. Appl. Arts Stud.* **2021**, *6*, 59–77.
16. Jahanmiri, F.; Parker, D. An overview of fractal geometry applied to urban planning. *Land* **2022**, *11*, 475. [CrossRef]
17. Ochoa, W.; Neto, A.; Junior, P.; Calabokis, O.; Ballesteros-Ballesteros, V. The Theory of complexity and sustainable urban development: A systematic literature review. *Sustainability* **2025**, *17*, 3. [CrossRef]
18. Chen, Y. Fractal modeling and fractal dimension description of urban morphology. *Entropy* **2020**, *22*, 961. [CrossRef] [PubMed]
19. Chen, Y. Scaling, fractals and the spatial complexity of cities. In *Handbook on Cities and Complexity*; Portugal, J., Ed.; Edward Elgar: Cheltenham, UK, 2021; pp. 176–194.
20. Telcs, A. Spectra of graphs and fractal dimensions I. *Probab. Theory Relat. Fields* **1990**, *85*, 489–497. [CrossRef]
21. Telcs, A. Spectra of graphs and fractal dimensions II. *J. Theor. Probab.* **1995**, *8*, 77–96. [CrossRef]
22. Griffith, D.; Arlinghaus, S. Urban compression patterns: Fractals and non-Euclidean geometries-inventory and prospect. *Quaest. Geogr.* **2012**, *31*, 21–28. [CrossRef]
23. Coxeter, H. *Non-Euclidean Geometry*; University of Toronto Press: Toronto, ON, Canada, 1965.
24. Greenberg, M. *Euclidean and Non-Euclidean Geometries: Development and History*, 2nd ed.; Freeman: San Francisco, CA, USA, 1980.
25. Falconer, K. *Fractal Geometry: Mathematical Foundations and Applications*; Wiley: New York, NY, USA, 2013.
26. Wu, J.; Jin, X.; Mi, S.; Tang, J. An effective method to compute the box-counting dimension based on the mathematical definition and intervals. *Results Eng.* **2020**, *6*, 100106. [CrossRef]
27. Cao, Z. Several Methods for Calculating and Estimating the Hausdorff Dimension. *Front. Comput. Intell. Syst.* **2023**, *5*, 28–32. [CrossRef]
28. Krause, K. *Taxicab Geometry*; Addison-Wesley: Menlo Park, CA, USA, 1963.
29. D'ambrosio, C.; Liberti, L. Distance geometry in linearizable norms. In Proceedings of the 3rd International Conference on Geometric Science of Information (GIS 2017), Paris, France, 7–9 November 2017; Nelsen, F., Barbaresco, F., Eds.; Springer: Cham, Switzerland, 2017; pp. 830–837.
30. Sowell, K. Taxicab geometry—A new slant. *Math. Mag.* **1989**, *62*, 238–248.
31. Krause, E. *Taxicab Geometry*; Dover: New York, NY, USA, 1975.
32. Reynolds, B. Taxicab geometry. *Pi Mu Epsil. J.* **1980**, *7*, 77–88.
33. Libeskind, S.; Jubran, I. Chapter 13: Taxicab geometry. In *Euclidean, Non-Euclidean, and Transformational Geometry*; Birkhäuser: Cham, Switzerland, 2024; pp. 569–605. [CrossRef]
34. Arlinghaus, S.; Nystuen, J. Street geometry and flows. *Geogr. Rev.* **1991**, *81*, 206–214. [CrossRef]
35. Calcagni, G. Geometry of fractional spaces. *Adv. Theor. Math. Phys.* **2012**, *16*, 549–644. [CrossRef]
36. Reinhardt, C. Taxi cab geometry: History and applications! *Math. Enthus.* **2005**, *2*, 38–64. [CrossRef]
37. Nagy, B. Calculating distance with neighborhood sequences in the hexagonal grid. In *Proceedings of Combinatorial Image Analysis: 10th International Workshop (IWCIA 2004), Auckland, New Zealand, 1–3 December 2004*; Klette, R., Žunić, J., Eds.; Springer: Berlin, Germany, 2005; pp. 98–109.
38. Brandts, J.; Křížek, M.; Somer, L. Regular tessellations of maximally symmetric hyperbolic manifolds. *Symmetry* **2024**, *16*, 141. Available online: https://www.mdpi.com/2073-8994/16/2/141 (accessed on 12 January 2025). [CrossRef]
39. Her, I. Geometric transformations on the hexagonal grid. *IEEE Trans. Image Process.* **1995**, *4*, 1213–1222. Available online: https://ieeexplore.ieee.org/stamp/stamp.jsp?tp=&arnumber=413166 (accessed on 12 January 2025). [CrossRef] [PubMed]
40. Grünbaum, B.; Shephard, G. *Tilings and Patterns*; Freeman: New York, NY, USA, 1987.
41. Kurlin, V. Mathematics of 2-dimensional lattices. *Found. Comput. Math.* **2024**, *24*, 805–863. [CrossRef]
42. Arlinghaus, S. Fractals take a non-Euclidean place. In *Solstice: An Electronic Journal of Geography and Mathematics*; Institute of Mathematical Geography: Ann Arbor, MI, USA, 2010; Volume XXI, Available online: http://deepblue.lib.umich.edu/handle/2027.42/58219 (accessed on 12 January 2025).
43. Frankhauser, P.; Pumain, D. Chapter 3: Fractals and geography. In *Machine Learning and the City: Applications in Architecture and Urban Design*; Carta, S., Ed.; Blackwell: London, UK, 2022; pp. 31–55.
44. Skums, P.; Bunimovich, L. Graph fractal dimension and the structure of fractal networks. *J. Complex Netw.* **2020**, *8*, cnaa037. [CrossRef]
45. Tharaniya, P.; Jayalalitha, G.; Raj, P.; Sundaravadivazhagan, B. *Advanced Fractal Graph Theory and Applications*; CRC Press: Boca Raton, FL, USA, 2024.
46. Kolyukhin, D. Study the accuracy of the correlation fractal dimension estimation. *Commun. Stat.-Simul. Comput.* **2024**, *53*, 219–233. [CrossRef]
47. Zhang, Z.; Song, Y.; Luo, P.; Wu, P. Geocomplexity explains spatial errors. *Int. J. Geogr. Inf. Sci.* **2023**, *37*, 1449–1469. [CrossRef]
48. Griffith, D.A.; Vojnovic, I.; Messina, J. Distances in residential space: Implications from estimated metric functions for minimum path distances. *GIScience Remote Sens.* **2012**, *49*, 1–30. [CrossRef]
49. Ord, J. Estimation methods for models of spatial interaction. *J. Am. Stat. Assoc.* **1975**, *70*, 120–126. [CrossRef]

50. Hadzieva, E.; Bogatinoska, D.; Gjergjeska, L.; Shuminoska, M.; Petroski, R. Review of the software packages for estimation of the fractal dimension. In *Proceedings of ICT Innovations 2015: Emerging Technologies for Better Living, Ohrid, Macedonia, 1–4 October 2015*; Loshkovska, S., Koceski, S., Eds.; Springer: Cham, Switzerland, 2016; pp. 201–211.
51. Arlinghaus, S. Fractals take a central place. *Geogr. Ann. J. Stockh. Sch. Econ.* **1985**, *67*, 83–88. [CrossRef]
52. Arlinghaus, S.; Arlinghaus, W. *Centrality and Hierarchy (Volume 1), Regular Lattices, Geometry, and Number Theory (Book 1)*; Spatial Synthesis; Institute of Mathematical Geography: Ann Arbor, MI, USA, 2005; Available online: https://deepblue.lib.umich.edu/bitstream/handle/2027.42/58273/SpatialSynthesisSummary.pdf?sequence=2&isAllowed=y (accessed on 13 December 2024).
53. Flores, J.; de la Fraga, L. Basic three-dimensional objects constructed with simplex meshes. In Proceedings of the 1st International Conference on Electrical and Electronics Engineering (ICEEE), Acapulco, Mexico, 8–10 September 2004; IEEE Catalog Number 04EXS65; IEEE Service Center: Piscataway, NJ, USA, 2004; pp. 166–171. Available online: https://ieeexplore.ieee.org/xpl/conhome/9798/proceeding (accessed on 12 January 2025).
54. Griffith, D. Eigenfunction properties and approximations of selected incidence matrices employed in spatial analyses. *Linear Algebra Its Appl.* **2000**, *321*, 95–112. [CrossRef]
55. Griffith, D. Extreme eigenfunctions of adjacency matrices for planar graphs employed in spatial analyses. *Linear Algebra Its Appl.* **2004**, *388*, 201–219. [CrossRef]
56. Chen, Y. Derivation of correlation dimension from spatial autocorrelation functions. *PLoS ONE* **2024**, *19*, e0303212. [CrossRef]
57. Arlinghaus, S. *Essays on Mathematical Geography—III*; Monograph 14; Institute of Mathematical Geography: Ann Arbor, MI, USA, 1991; Available online: http://deepblue.lib.umich.edu/handle/2027.42/58219 (accessed on 12 January 2025).
58. Chen, Y. Fractal texture and structure of central place systems. *Fractals* **2020**, *28*, 2050008. [CrossRef]
59. Griffith, D.; Sone, A. Trade-offs associated with normalizing constant computational simplifications for estimating spatial statistical models. *J. Stat. Comput. Simul.* **1995**, *51*, 165–183. [CrossRef]
60. Boots, B.; Royle, G. A conjecture on the maximum value of the principal eigenvalue of a planar graph. *Geogr. Anal.* **1991**, *23*, 276–282. [CrossRef]
61. Maćkiewicz, A.; Ratajczak, W. Towards a new definition of topological accessibility. *Transp. Res. Part B Methodol.* **1996**, *30*, 47–79. [CrossRef]
62. Xie, F.; Levinson, D. Measuring the structure of road networks. *Geogr. Anal.* **2007**, *39*, 336–356. [CrossRef]
63. Bunimovich, L.; Skums, P. Fractal networks: Topology, dimension, and complexity. *Chaos Interdiscip. J. Nonlinear Sci.* **2024**, *34*, 042101. [CrossRef] [PubMed]
64. Park, R.; Burgess, E. *The City*; The University of Chicago Press: Chicago, IL, USA, 1925.
65. Arlinghaus, S.; Griffith, D. Mapping it out! A contemporary view of Burgess's concentric ring model of urban growth. In *Solstice: An Electronic Journal of Geography and Mathematics*; Institute of Mathematical Geography: Ann Arbor, MI, USA, 2010; Volume XXI, Available online: www.mylovedone.com/image/solstice/win10/ArlinghausandGriffith.html (accessed on 12 January 2025).
66. Thrasher, F. Chicago's Gangland Map. 1923. Available online: https://www.loc.gov/item/2013586117/ (accessed on 28 November 2024).
67. Arlinghaus, S.; Nystuen, J. Geometry of boundary exchanges: Compression patterns for boundary dwellers. *Geogr. Rev.* **1990**, *80*, 21–31. [CrossRef]
68. Arlinghaus, S.; Arlinghaus, W. The fractal theory of central place hierarchies: A Diophantine analysis of fractal generators for arbitrary Löschian numbers. *Geogr. Anal.* **1989**, *21*, 103–121. [CrossRef]
69. Arlinghaus, S.; Griffith, D. Eigenvalue fractal geometry: An alternative approach to fractal generation. In *Solstice: An Electronic Journal of Geography & Mathematics*; Institute of Mathematical Geography: Ann Arbor, MI, USA, 2014; Volume XXV, Available online: https://deepblue.lib.umich.edu/bitstream/handle/2027.42/108255/ArlinghausGriffithVolXXVNo1.pdf (accessed on 12 January 2025).
70. Batty, M.; Longley, P.; Fotheringham, S. Urban growth and form: Scaling, fractal geometry, and diffusion-limited aggregation. *Environ. Plan. A* **1989**, *21*, 1447–1472. [CrossRef]
71. Abid, R. Fractal analysis of urban growth in complex systems. *Edelweiss Appl. Sci. Technol.* **2024**, *8*, 2133–2140. [CrossRef]
72. Balestro, V.; Martini, H. Chapter 3: Minkowski geometry—Some concepts and recent developments. In *Surveys in Geometry I*; Papadopoulos, A., Ed.; Springer: Cham, Switzerland, 2022; pp. 49–95. [CrossRef]
73. Fu, M.; Chen, Y. Characterizing the spatio-temporal variations of urban growth with multifractal spectra. *Entropy* **2023**, *25*, 1126. [CrossRef] [PubMed]